Iranian Journal of Geophysics, Vol 16 No 4, 2023, Page 37 – 52 (Research Article)
DOI: 10.30499/ijg.2022.295242.1343

Evaluation of geothermal energy potential of parts of the Middle Benue trough Nigeria: aeromagnetic and aeroradiometric approach

Ikumbur Emmanuel Bemsen [1], Onwuemesi Ajana Godwin[2], Anakwuba Emmanuel Kenechukwu[3], Chinwuko Augustine Ifeanyi[4] and Usman Ayatu Ojonugwa [5*]

[1] Assistant Professor, Department of Geology, Benue State Polytechnic, Ugbokolo, Nigeria
[2] Professor, Department of Applied Geophysics, Nnamdi Azikiwe University, Awka, Nigeria
[3] Professor, Department of Applied Geophysics, Nnamdi Azikiwe University, Awka, Nigeria
[4] Associate Professor, Department of Applied Geophysics, Nnamdi Azikiwe University, Awka, Nigeria
[5] Assistant Professor, Department of Applied Geophysics, Faculty of Physical Sciences Alex Ekwueme Federal University, Ndufu-Alike, Ikwo, Nigeria

(Received: 15 July 2021, Accepted: 8 May 2022)

Abstract

Geothermal energy potential investigation over parts of Middle Benue Trough, Nigeria, has been evaluated using aeromagnetic and aeroradiometric datasets. The input data consists of nine aeromagnetic and aeroradiometric sheets, respectively. The aeromagnetic data was assembled and digitized; this produces a total magnetic intensity anomalous map (TMI). Similarly, the radiometric data were contoured to produce maps for the three radiometric elements of K, Th, and U. The rose diagram showed that the structural trend in the study area is trending NE-SW and the minor ones are trending E-W and NNE-SSW directions. The radiometric heat model reveals areas of high and low geothermal gradient. The results of quantitative interpretation reveal that the depth to anomalous magnetic sources (the sedimentary infilling) ranges between 0.76 and 4.46 km; while the depth to centroid ranges between 7.29-19.6 km. The Curie point depth (CPD) corresponds to the depth to the bottom of the anomalous magnetic source. The CPD varies from 12.70-37.22 km, the geothermal gradient varies between 15.58-45.67^{0C}/km, and the geothermal heat flow varies from 38.9-114.17 mW/m2. The two dimensional structural models show uplifted crust and mantle in some areas due to magmatic intrusions, which gave rise to low CPDs (12 to 28 km), which resulted in high geothermal heat flow values (60 to 115 mW/m2). The geothermal heat flow values around Kwolla, Shendam, Lafia, Akiri, Ibi, and Wukari South fall between 60 and 100 mW/m2, which is the suitable standard for geothermal potentiality.

Keywords: Curie depth, geothermal energy, geothermal heat, radiometric heat, spectral analysis

*Corresponding author: ayatu.ao@funai.edu.ng

1 Introduction

One of the biggest oil and gas producers in the world is Nigeria, and the major source of energy in the country is mainly hydrocarbons. Despite this fact, the basic problem facing Nigerian energy sector is an increase in demand for energy without a corresponding increase in generation of more energy. The population of Nigeria is seriously increasing and the demand for energy is also on the increase without a plan to generate more energy to meet people's demands. Again, the present call to save our environment from pollution has made researchers start thinking toward a cleaner source of energy. One of the sustainable ways to do this is through geothermal energy generation. Geothermal energy is an abundant, secure, unpolluted, and clean source of energy, which originated from the formations in a sedimentary basin and from radioactive decay of elements within the basement complex rocks (Abraham et al, 2014; Sedara and Joshua 2013). Moreover, geothermal studies have not received sufficient consideration across Nigeria as such; there is a gap in the crustal temperature record and this necessitates this study.

Geothermal energy is a viable source of energy in the most developed countries in the world. This geothermal energy is normally revealed around the surface of the terrestrial and they exist like volcanoes and fumaroles (dumps where volcanic gases are taped), hot springs, altered grounds, steaming grounds, and geysers, (Ochieng, 2013; Yamano, 1995). The Geothermal energy which exists closer to the earth's surface can the tapped by drilling about 3 km wells. The narrow heat sources are in most situations accredited to volcanic action which are usually connected to plate boundaries, and other geodynamic surroundings (Salako et al., 2020; Ochieng, 2013). The vital part of a geothermal structure include: heat flow, cap rock recharge regime, and permeable reservoir. Multiple geoscientific disciplines such as geophysics, geology, and geochemistry are usually hired in the geothermal exploration.

The study area was chosen because of the evidence of hot springs in and near the study area. From several researches, it is found that one of the hottest springs (53.5^0C) in the area is situated close to Akiri, and another well-known Nigerian warm spring is Wikki warm spring (32^0C), which flows from Gombe Sandstone in Yankari Game Reserve (Abraham and Nkitnam 2017; Salem, and Fairhead, 2011; Stampolidis et al 2005). There is another hot spring located around the Northern part of Benue Trough, near the study area, within a massive tectonic arrangement. Lamurde anticline, near Numan and is called Ruwan Zafi. The water of the spring is heated by geothermal gradient on its way from unknown depths, in an unconfined sandstone aquifer (Anudu et al 2014; Beamish and Busby, 2016; Kasidi and Nur, 2013; Okubo et al, 1985; Ross et al 2006).

The study aim at investigating geothermal energy potentials of parts of Middle Benue Trough using integrated spectral analysis of aeromagnetic data and radiometric data. This aim is achieved through evaluation of the Curie point depths and succeeding geothermal parameters; delineation of the structural trends and attributes in the study area; production of a radiometric heat map; compare the radiometric heat and the geothermal heat flow; delineate of areas with geothermal energy potentials.

2 Location and geology

The surveyed area is bounded within latitudes 7^030^1 N to 9^000^1 N and longitudes 8^030^1E to 10^000^1E of the middle part of the Benue Trough of Nigeria (Figure. 1) which is an inland basin In Nigeria. The Middle Benue Trough connected the lower and upper parts of the Nigeria Benue Trough. It forms a long stretched arm of the Central African Rift System. The basin chronologically was formed around the early Cretaceous which is marked by

rifting of the Central West African basement (Obaje, 2009; Offodile, 1980). The Benue Trough is a linear Northeast to Southwest (NE-SW) trending structure categorized by the occurrence of thick sedimentary infilling of diverse composition which chronologically ranges from Albian to Maastrichtian (Obaje, 2009; Telford et al, 1990)

The investigation area is overlaying younger granites, volcanic rocks, and crystalline basement rocks (NGSA, 2009; Offodile, 1989) (Figure. 1). There are two groups of the crystalline basement rocks of Nigeria, namely; the Migmatite-Gneiss Complex and the Older Granites. Much of the investigated area is underlined by the Cretaceous sedimentary rocks and it comprises the following formation; Asu River Group, the Awe Formation, Keana Formation, Makurdi Formation, Ezeaku Formation, Awgu Formation, and Lafia Formation (Figure. 1). The marine sediment of the Asu-River group is Albian in age and started the sedimentary infilling in the Middle Benue Trough (NGSA, 2009). The rocks are greatly deformed during the Santonian tectonic episode (about 86 Ma) to produce several folds, faults, and uplifts, which generally trend in the NE-SW direction, parallel to the trough margin (Benkhelil, 1989; Burke et al, 1972).

There is a regression phase in the Awe Formation comprising intermediate bed surfaces of sandstones and carbonaceous shales. The formation overlies the Asu River Group (Burke and Whiteman, 1973; Cratchley and Jones, 1965; Obaje, 2009). The Awe Formation overlay continental fluvial sands of the Keana Formation. Both the Awe and the Keana formations are overlaid by the Ezeaku Formation which consists of calcareous shales, micaceous fine to medium grained sandstones, and shelly limestones in the Middle Benue Basin (Cratchley and Jones, 1965). Locally, the shales grade into the predominantly fluvial cross bedded sandstones of the Makurdi Formation (Figure. 1). The Ezeaku Formation is overlain by the Awgu Formation in the Lower and Middle Benue basins. This consists of a system of fossiliferous black shales and limestones in the Abakiliki Basin. The top parts of the Ezeaku Formation and the marine successions of the Awgu Formation were deposited during the Late Cenomanian to Coniacian transgressive cycle (Offodile, 1976).

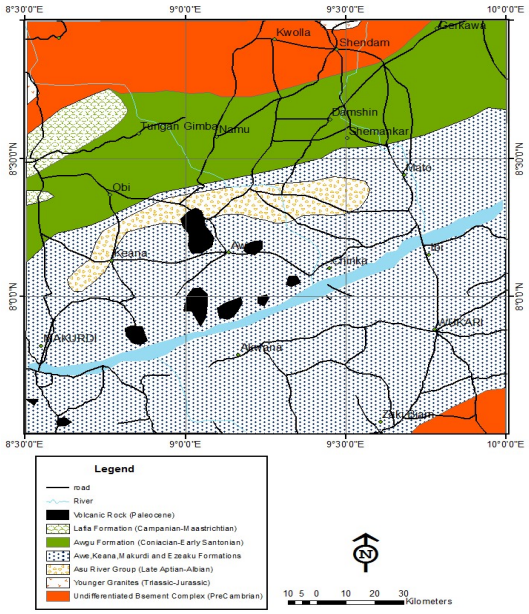

Figure 1. Geologic map of the study area.

3 Methodology

Both the aeromagnetic and aeroradiometric data sets were obtained through purchase from Nigerian Geological Survey Agency (NGSA) in digitized form. Nine aeromagnetic maps covering the survey area are assembled (figure. 2) and contoured to yield total magnetic intensity (TMI) anomalous map. The anomalous (TMI) map contains both the regional and residual anomalous field and for we to interpret the local field, we separate the field by fitting in a linear trend surface using the multiple regression techniques as guided by equation (1) and (Likkason, 1993).

$$p(x, y) = ax + by + c \quad (1)$$

Where, a, b and c=constants; x and y=distances in x and y coordinates;
$p(x, y)$=the magnetic value at x and y coaxis.

Similarly, nine radiometric data sheets were acquired, assembled, and contoured to produce one map for each of the three radiometric elements, potassium (K), thorium (Th), and Uranium (U). From the heat calculations, a single radiometric heat map was produced (Figure. 16). The Fourier Transform is the mathematical tool deployed for quantitative analysis.

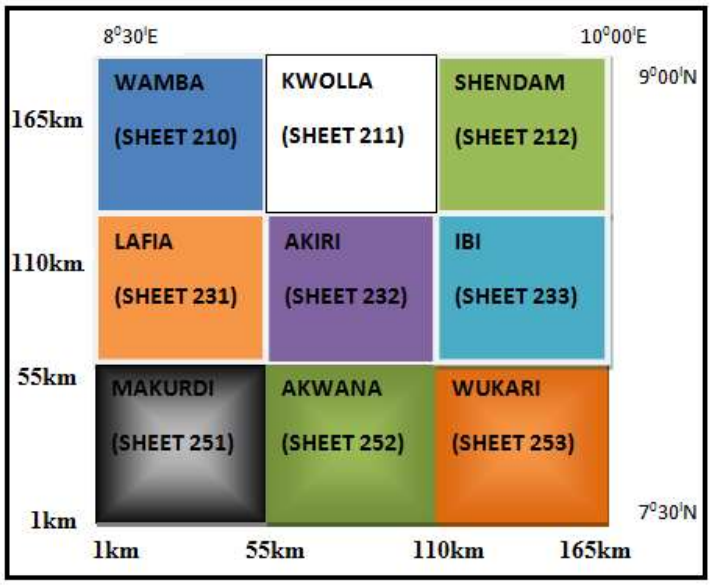

Figure 2. The composite aeromagnetic map

Fourier series is summarized by (Nwankwo and Abayomi, 2017) as:

$$f(x) = a_0 + \sum_{n=1}^{\infty} \left(a_n \cos \frac{2n\pi x}{L} + b_n \sin \frac{2n\pi x}{L} \right) \quad (2)$$

Where $Y_i(x)$=the amplitude at a point
$x_i x_i$ = position thedistance along x axis
L=length of the anomalous cross-section (or wavelength of the sampling distance)
n=partial wave harmonic number (or the frequency of the partial wave (Note: n should not exceed the Nyquist frequency; Nyquist frequency ≈ L/2. IfNyquist frequency is exceeded; there will be a repetition of transformed data)
N=the data points
(Where a_n and b_n are coefficients of the first harmonic or partial amplitudes)
i=0, 1, 2, 3, ..., n

a_n=real component of the amplitude spectrum
b_n=imaginary component of the amplitude spectrum } Partial Amplitude

The Partial amplitudes (a_n and b_n) are calculated using the following equations:

(3)

$a_n = 2/N \sum_{n=1}^{N} Yi \cos \frac{2n\pi x}{L}$ (Davis, 1972)

(4)

$b_n = 2/N \sum_{n=1}^{N} Yi \sin \frac{2n\pi x}{L}$ (Davis, 1972)

Hence, the main amplitude spectrum (An) is given by:

$An = \sqrt{a_n 2 + b_n 2}$ (5)

The graphs obtained from a plot the natural logarithms of the amplitude (A_n) against frequency (n). A linear segment was drawn from the low frequency portion of the spectral to enable us to take a gradient of the linear segments and hence calculate the basal depth using the equation as stated by (Bello et al, 2017; Nwankwo and Shehu, 2015), given as;

$Zt = -ML/2\pi$ (Blakely, 1988) (6)

Where Zt=basal depth (depth to top)
M=linear section gradient
L=length of the anomalous cross-section.

To obtain depth to Curie point; the first step is to estimate the depth to the centroid (Z_o) of the magnetic anomalous source. The second step is the estimation of the depth to the top (Z_t) of the magnetic anomalous source, then, the basal depth (Z_b) of magnetic anomalous sources in the investigated area is presumed to be Curie point depth (CPD) (Bansal et al, 2013; Bhattacharyya and Leu, 1975; Okubo et al, 1985; Nwankwo and Abayomi, 2017). The basal depth (Z_b) of the magnetic anomalous source is computed using the equation below,

$Zb = 2Zo - Zt$ (7)

Where, Zo is the centroid depth (depth to centre of anomalous source),
Zt is the depth to top of magnetic source (sedimentary thickness) and
Zb is the basal depth (depth to the bottom of anomalous source).

The geothermal gradient and heated is computed by the formula (Okubo et al, 1985).

$Q = \lambda dT/dZ$ (8)

Where Q=geothermal heat flow
λ=coefficient of thermal conductivity (given as 2.5 W/m^{0}C).

In this equation, we presumed that the temperature direction is vertical and that the gradient of the temperature dT/dz is constant as such there should be no loss or gain above the crust and below the Curie point depth. According to (Blakely, 1988; Ikechukwu et al, 2015; Tanaka et al, 1999), the Curie temperature (θc) was gotten from the Curie point depth (Z_b) and the thermal gradient $^{dT}/_{dZ}$ and stated in (equation 9, 10 and 11);

$\theta c = \{dT/dZ\}$Zb (9)

In addition to the above, from equation (10) and (11) and work of Ojonugwa et al (2018) is the connection between the Curie point depth (Z_b) and the heat flow (Q) as follows;

$Q = \{\theta c/$Zb$\}\lambda$ (10)

The equation reveals that there is an inverse relationship between Curie point depth and heat flow, (Cratchley and Jones, 1965; Stampolidis et al, 2005; Sedara and Joshua, 2013). The Curie point temperature of 580^{0}C and thermal conductivity of 2.5 Wm/^{0}C which is average values for igneous rocks was used as a model in this study and supported by Obaje et al, 2004; Nwankwo and Shehu (2015).

Equation (10) was utilized to compute the geothermal gradient of the region as the ratio of Curie temperature to Curie point depth.

Hence we have: $\frac{dT}{dZ} = \frac{\theta c}{Zb}$ (Salem and Fairhead, 2011; Ross et al, 2006; Yamano, 1995) (11)

Where dT/dT is geothermal gradient, Zb is the basal depth and Θc is the standard Curie point temperature of 580^{0}C

The radioactive heat model is computed from radiometric data as shown the equation:

$A(\mu W/\text{m3}) = \rho(0.0952Cu + 0.0256CTh + 0.0348Ck)$ (12)

Where A=radiometric heat (in μW/m^3)ρ=density of rock in kg/m^2 (adopted from Telford et al (1990)

C_u, C_{Th} and C_k are the concentrations of uranium, thorium and potassium (in ppm for C_u and C_{Th}, and % for C_k) respectively.

The concentrations of the three (3) element gotten from the radiometric data is in a way that covers the exact position where nine (9) sheets were gotten and processed (Beamish and Busby, 2016).

4 Results and discussion

The TMI (Figure. 3) has a total magnetic intensity value ranging from 33340 nT to 33300 nT. Higher magnetic intensity is found in the northern, north central, western, southwestern, and southern parts of the study area; while lower magnetic intensity values (shown in blue) are found in the northwest, northeast, central and south-eastern regions (Figure. 3a).

The investigated area is categorized by tightly spaced linear to sub-linear contours which recommend faulting or fracturing, which may probably be a migrating pathway for fluid or geothermal (Figure. 3a and b). Generally, the trend of the contour anomalous TMI map is northeast (NE) to southwest (SW) direction and it is in conformity with the trend of structures in the Benue trough. The residual anomalous field map (Figure. 3b) similar trend of fibers to those of the TMI (Figure. 3a). The oval contour observed in the area reveals the presence of magnetic anomalous bodies Figure. 5.

(a)

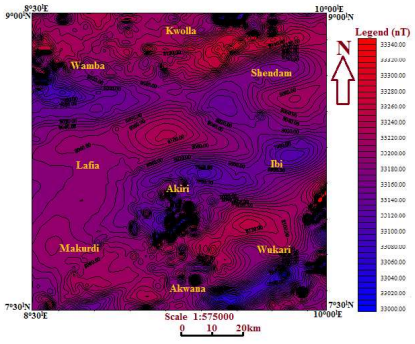

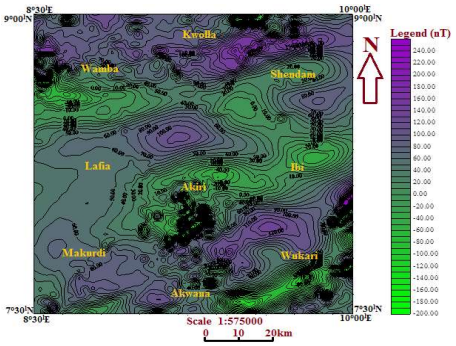

(b)

Figure 3. (a) Total Magnetic Intensity (TMI) Map (Contour Interval=10 nT) (b) Residual Anomalous Map (Contour Interval=10 nT).

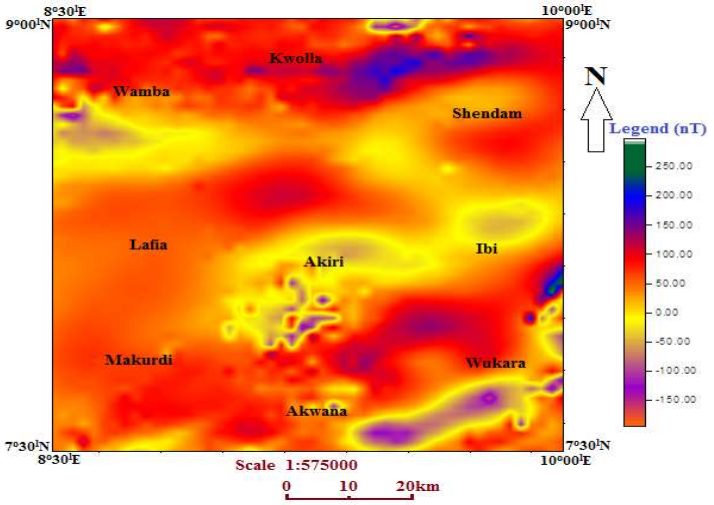

Figure 4. Upward Continuation Model of the investigated area.

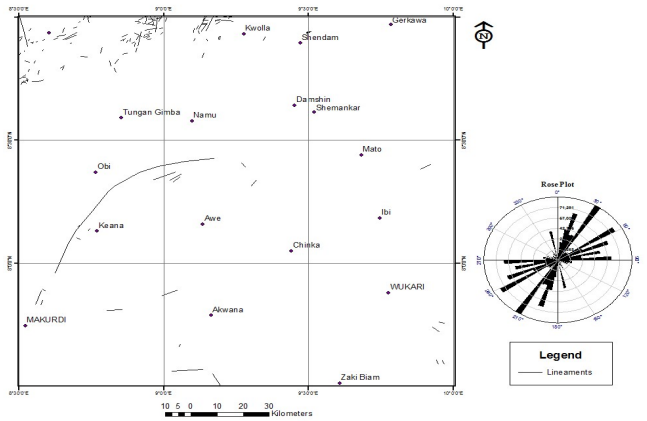

Figure 5. Lineament map of the study Area with Rose Diagram.

The residual anomaly map reveals that the contour lines are broadly spaced in the NW, West, and SW parts of the area, this signposts that there are thicker sediments in those regions (Wamba, Lafia, and Makurdi), implying that the basal depth is higher in these areas relative to the areas where there are closely spaced contours which suggests shallow sedimentary infilling. Figure. 3b also shows positive magnetic anomalies in areas like Wamba, Lafia, and Makurdi which suggests deeper depths in such areas, while areas around Shendam, Ibi, and Akiri show negative anomalies which indicate shallower depths to magnetic bodies.

Upward continuation was applied to suppress the effects of small scale features near the surface and also to reduce topographic effects. The Upward Continuation map of the study area (Figure. 4) shows areas with the highest magnetic intensity in blue color (near Kwolla). Wamba (north), Lafia, Makurdi and Akwana have higher intensity, while Akiri, Ibi, Wukari, and Wamba (south) have lowest intensities.

The enhance upward continuation map superimposed on our structural map (Figure. 4), was used to pick the basic trend of the structures and then plotted in a rose diagram (Figure. 5) (Magnetic lineament map and Rose Diagram) show that the main trend of the lineaments is NE-SW, while minor ones trend E-W and NNE-SSW directions. The major anticline recognized on the model map in figure. 5 is in conformity with the Keana Anticline, trends NE-SW and it covers parts of the northeast of Makurdi via north of Keana to the north of Awe (Akiri). Three minor anticlines close to the major one with an axis trending NE-SW also occur. The geological structures (lineaments, dykes and faults) reveals are relatively long signifying regional structure trends (Biswas et al., 2017; Anudu et al, 2014; Nwankwo and Shehu, 2015). These main structural trends (NE-SW and E-W) agree with the magnetic trend results (Figure. 3a and 3b). Quantitative analysis started by drawing seven (7) profile lines, namely AA^{I}-GG^{I} and it was drawn in the northwest-southeast (NW-SE) direction, and used for detailed interpretation (Figure. 6).

Using the Microsoft Excel package, the graphs of magnetic intensity against distance on the profiles were drawn to show the nature of magnetic anomalies found in the area (Figure. 7).

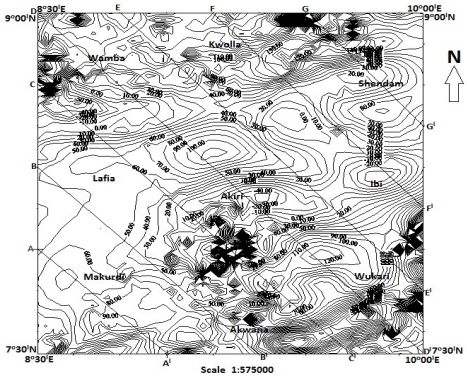

Figure 6. Residual Anomalous Map Showing the Profile Lines (Contour Interval=10 nT).

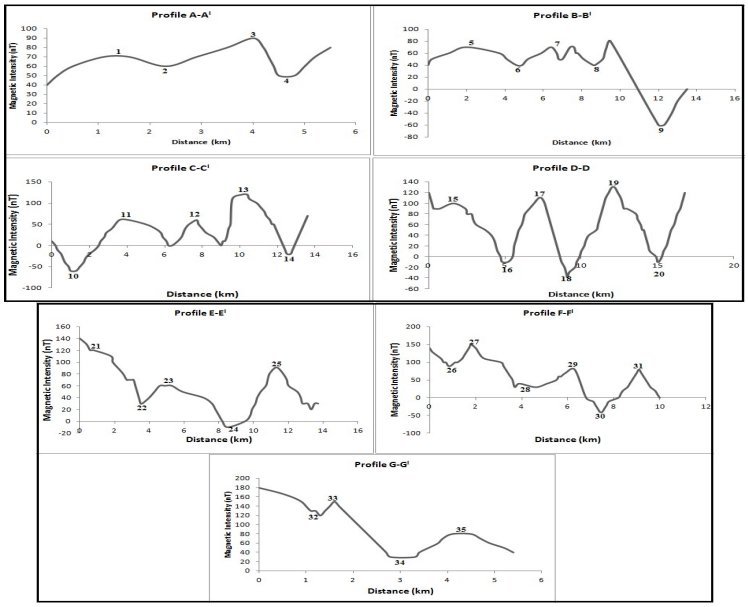

Figure 7. Magnetic anomaly graphs shown on profiles A-A^{l} to G-G.^{l}

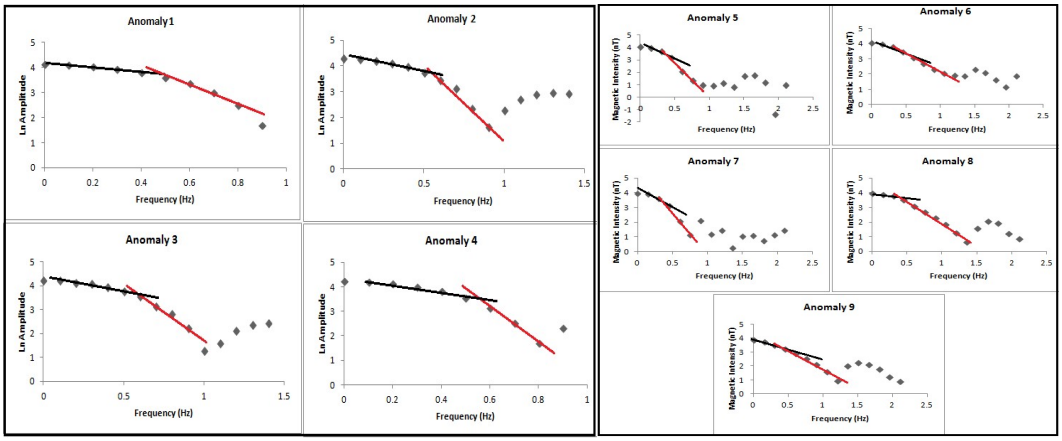

Figure 8. (a): Spectral graphs of profile A-A^{l} and B-B.^{l}

Table 1. Computed Curie Point Depths and Geothermal Parameters gotten from Fourier Analysis.

Anomaly	Depth to the Top (km)	Depth to the Centroid (km)	Curie Point Depth (km)	Geothermal gradient	Heat Flow(mW/m^2)
1	1.34	12.21	23.08	25.1230	62.8250
2	1.72	13.76	25.80	22.4806	56.2016
3	1.27	13.09	24.91	23.2838	58.2096
4	1.73	12.89	24.05	24.1164	60.2911
5	2.41	16.51	30.61	18.9481	47.3701
6	1.51	14.49	27.47	21.1139	52.7849
7	4.46	16.38	28.30	20.4947	51.2368
8	2.16	13.51	24.86	23.3307	58.3266
9	2.32	15.67	29.02	19.9862	49.9655
10	2.49	16.31	30.13	19.2499	48.1248
11	2.80	14.12	25.44	22.7987	56.9969
12	2.08	10.92	19.76	29.3522	73.3806
13	1.54	15.87	30.20	19.2053	48.0133
14	3.09	15.85	28.61	20.2726	50.6816
15	3.62	15.76	27.90	20.7885	51.9713
16	2.30	16.18	30.06	19.2947	48.2369
17	2.27	11.31	20.35	28.5012	71.2531
18	1.98	19.60	37.22	15.5830	38.9576
19	2.57	18.11	33.65	17.2363	43.0906
20	2.14	11.27	20.40	28.4314	71.0784
21	2.57	12.62	22.67	25.5845	63.9612
22	2.28	19.24	36.20	16.0221	40.0553
23	2.14	17.38	32.62	17.7805	44.4513
24	1.91	18.41	34.91	16.6142	41.5354
25	1.73	17.76	33.79	17.1648	42.9121
26	1.94	10.21	18.48	31.3853	78.4632
27	1.72	18.27	34.82	16.6571	41.6427
28	2.11	11.34	20.57	28.1964	70.4910
29	2.31	9.29	16.27	35.6484	89.1211
30	2.18	18.75	35.32	16.4213	41.0532
31	1.88	7.29	12.70	45.6693	114.1732
32	1.08	12.39	23.70	24.4726	61.1814
33	0.76	11.18	21.60	26.8519	67.1296
34	2.27	9.36	16.45	35.2584	88.1459
35	2.19	10.19	18.19	31.8857	79.7141
Average	2.14	14.21	26.29	23.5772	58.9436

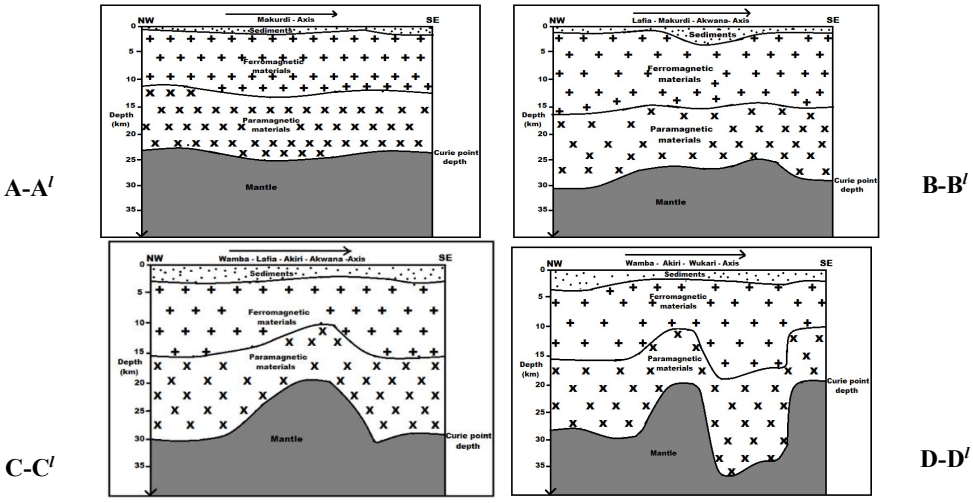

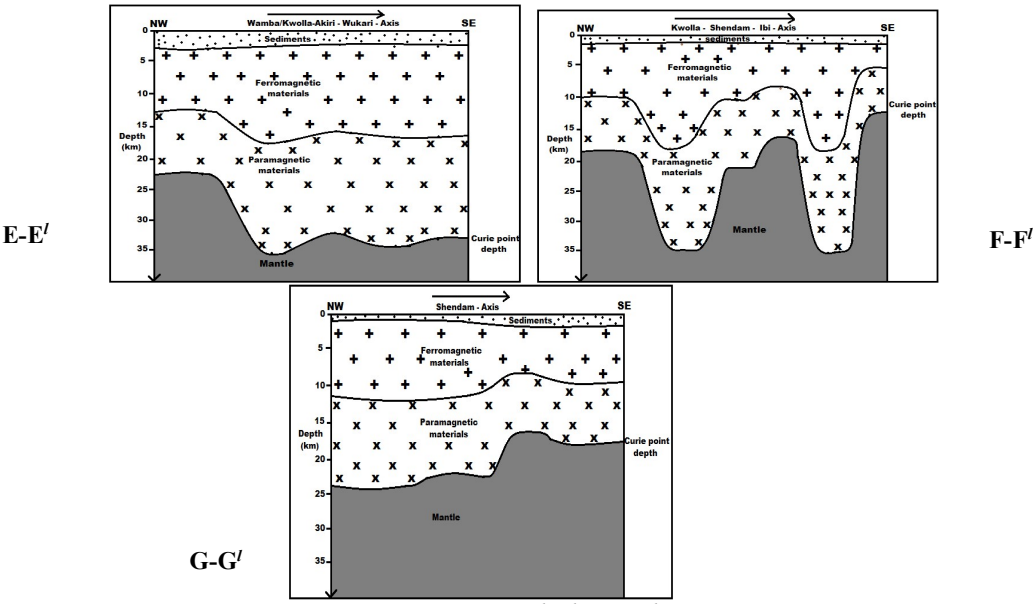

Figure 9. Structural modeling along Profile $A^{/}$-$A^{/}$ to G-$G^{/}$ within the study area.

Spectral graphs were then obtained from the profiles by plotting the values of magnetic intensity against frequencies. The graphs of amplitude against frequencies were plotted for various profiles (A–$A^{/}$ to G-$G^{/}$). There are two segmented lines in each: the first segment is used to compute depth-to-centroid (Zo) representing depths to deeper sources, while the second line segment gives the depth-to-top of magnetic anomalous sources which shows shallower depths to magnetic sources.

The gradient of each of the segmented lines was computed the basal depth was (Zo and Zt) (Figure. 8a to 8g).

From the result obtained rom the Fourier Transform analysis calculation, a two dimension structural model was constructed to reveal the configuration of the basin. We pick the depth calculation from the analyzed profile line and the two dimensional structural models were constructed to show the calculated depths (depth-to-top or sedimentary thickness, depth-to-bottom or Curie point depth) and estimated depth to the Mantle plume. The structural models show the sedimentary thickness, magnetic crust which hosts the Ferromagnetic materials and Paramagnetic materials, and the Mantle (Figure. 9). The Ferromagnetic materials have high magnetic susceptibility, while the Paramagnetic materials have low magnetic susceptibility. In the Mantle, there are no magnetic materials because they lost their magnetic properties due to high temperature.

The depth to the top of the anomalous magnetic bodies (Zt) around Shendam, Ibi, Akiri, and Wukari is shallow (Figure 10a and b), northeast to the south-eastern part of the survey area, while higher values of Zt are observed at Wamba, Lafia, Akiri, and Makurdi. The 3D Curie depth map (Figure. 11a and b) show that the regions around north-west and north-central (Wamba and Kwolla) and east to the south-east (Ibi and Wukari) have higher Curie point isotherm depths ranging from 28.30 km to 37.22 km, while lower depths ranging from 12.70 km to 27.90
km are found around the northern part of Wamba and Kwolla, Shendam (NE), Akiri (Central), Lafia and Makurdi (SW) and Wukari south (SE). Yamano (1995) made a statement that shallower Curie point depths are dependable with high heat flow values as observed in back arc, and young volcanic regions. As regards, this statement, the zone of shallower Curie point

depth of 12.70 km to 27.90 km has a geothermal potential that can be exploited.

Again, 3D maps of the Geothermal gradient model (Figure. 12a and b) of the study area reveal at areas around Lafia, Akiri, the northern part of Wamba, and Kwolla, Shendam, Ibi, Makurdi, and the southern part of Wukari have high values of geothermal gradient. From the depth calculation (Table 1), the geothermal gradient and curie isotherm depth (Figure. 13) show an inverse relationship. An area with high heat flow and high geothermal gradient agrees with an area with low curie isotherm depth and verse versa. The regression coefficient gotten is y= 2.5x + 0.0002 for the relation between the geothermal gradient and heat flow.

The radiometric map (Figure. 14a) shows a high concentration of potassium (K) around Wamba, Kwolla, and part of Shendam (in the northern part), between Ibi and Wukari, and Akwana. Low con centration of Potassium is prevalent around Lafia, Makurdi, part of Shendam, Akiri, and part of Wukari. Shales, Sandstones, and Granite (especially Feldspar) are rocks related to high potassium activity. The Thorium content map (Figure. 14b) reveals a high concentration of Thorium around Wamba, Kwolla, Shendam, Lafia, Akiri, Ibi, and Wukari south. Low concentrations of Thorium are predominant around Makurdi, Akwana, Akiri, and Wukari. Mineralization associated with thorium includes basement granitic rocks, migmatite, shales, and clay. The Uranium content map (Figure. 14c) reveals a high concentration of Uranium around Lafia, Akiri, Ibi, Akwana, south of Wukari, and Makurdi north. A low concentration of U is found around Kwolla, Shendam, Wamba, Wukari, and Makurdi south.

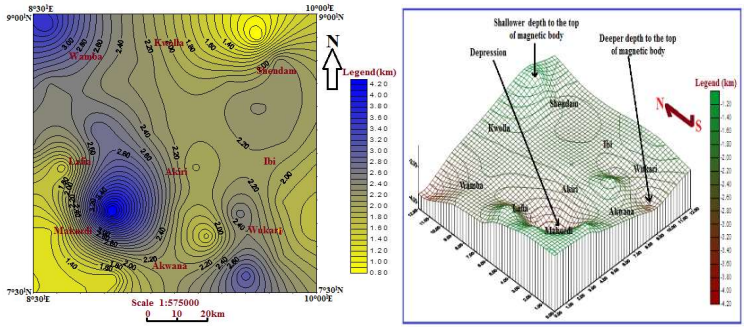

Figure 10. (a) Model map of depth to top of magnetic anomalous sources (Contour interval~0.1 km) (b) 3D view of depth to the top within the study area.

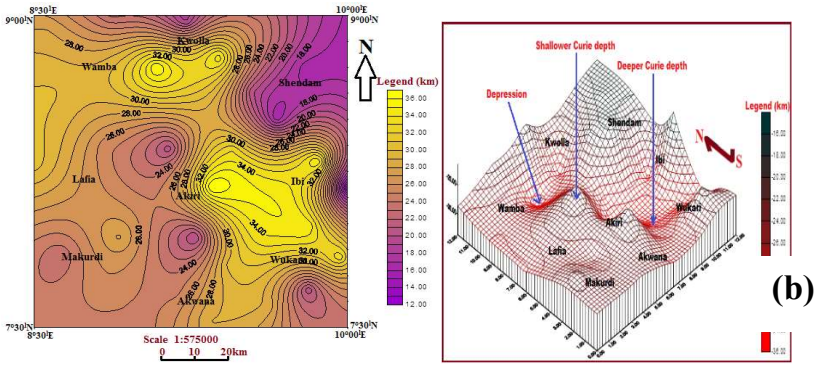

(a) **(b)**

Figure 11. (a) Model map of Curie Depth (Contour interval~1.0 km) (b) 3D view of Curie point depth.

(a)

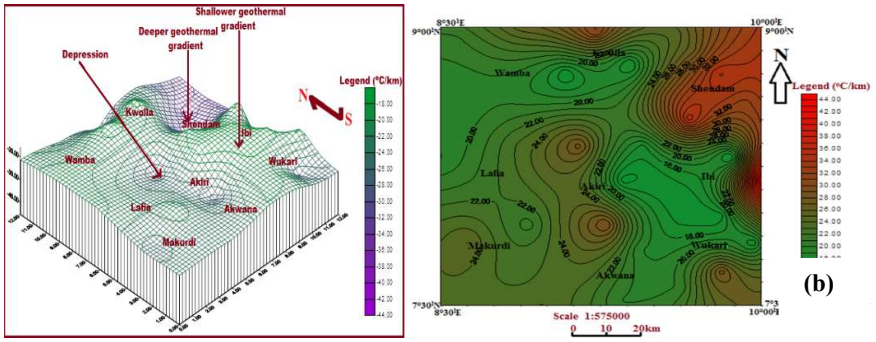

(b)

Figure 12. (a) Map of Geothermal gradient (Contour interval~1.0°C/km) (b) 3D view of geothermal gradient.

(a)

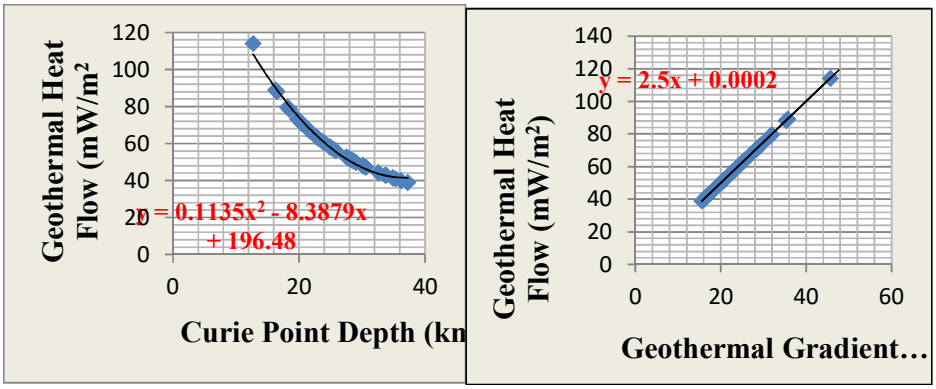

(b)

gure 13. (a) Relationship between Curie point Depth and Heat Flow (b) Relationship between Geothei gradient and Heat flow.

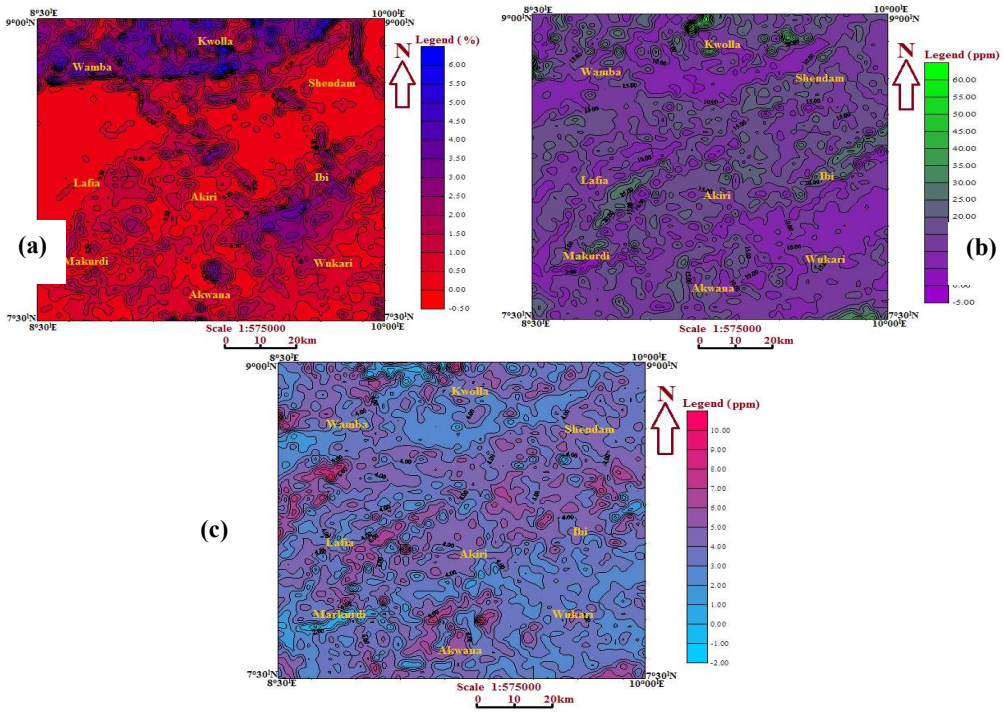

Figure 14. (a) Potassium Data Map (contour Interval≈0.5%) (b)Thorium Data map (contour Interval≈5.0 ppm) (c) Uranium Data map (contour Interval≈1.0 ppm).

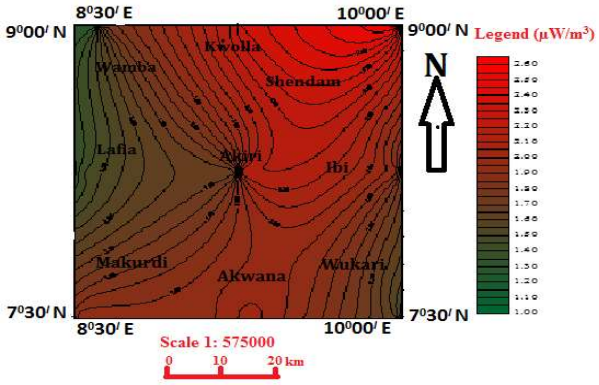

Figure 15. Radiometric Heat Map Contour Interval≈0.05 μW/m^3.

Shales, clay, and basement complex rocks (such as granite and migmatite) are associated with uranium mineralization.
A high concentration of radiometric heat has the highest occurrence around Wamba, Kwolla, Shendam, Akiri, Ibi, Makurdi, and Akwana. These areas are the hot spots that are potential geothermal areas. Low concentrations are found around Wamba south, Kwolla south, Lafia, Shendam north, and Wukari north (Figure. 15). The areas of high radiometric heat concentration correspond with the areas with low Curie point depth, high geothermal gradient, and high geothermal heat flow (Figure. 10, 11, and 12 respectively).

5 Conclusion

Qualitatively, the TMI reveals that the magnetic intensity value ranges from 780 nT to 8240 nT. The main trend of the lineaments is NE-SW, while minor ones trend in E-W and NNE-SSW directions. The major anticline recognized on the model map is in conformity with the Keana The anticline that trends NE-SW and it covers parts of the northeast of Makurdi via north of Keana to the north of Awe (Akiri). The depth to the top of the anomalous magnetic bodies (Zt) around Shendam, Ibi, Akiri, and Wukari is shallow around the northeast to the south-eastern part of the survey area, while higher values of Zt are observed at Wamba, Lafia, Akiri, and Makurdi. The 3D Curie depth shows that the regions around northwest and north-central (Wamba and Kwolla) and east to the south-east (Ibi and Wukari) have higher Curie point isotherm depths ranging from 28.30 km to 37.22 km, while lower depths ranging from 12.70 km to 27.90 km are found around the northern part of Wamba and Kwolla, Shendam (NE), Akiri (Central), Lafia and Makurdi (SW) and Wukari south (SE).

3D maps of the geothermal gradient model reveal at areas around Lafia, Akiri, the northern part of Wamba and Kwolla, Shendam, Ibi, Makurdi, and the southern part of Wukari have high values of geothermal gradient. The geothermal gradient and curie isotherm shows an inverse relationship. An area with high heat flow and high geothermal gradient agrees with an area with low curie isotherm depth and verse versa.

The radiometric results show a high concentration of potassium (K) around Wamba, Kwolla, and part of Shendam (in the northern part), between Ibi and Wukari, and Akwana. Low concentration of Potassium is prevalent around Lafia, Makurdi, part of Shendam, Akiri, and part of Wukari. Shales, Sandstones, and Granite (especially Feldspar) are rocks related with high potassium activity. There is a high Thorium concentration around Wamba, Kwolla, Shendam, Lafia, Akiri, Ibi, and Wukari south. Low concentrations of Thorium are predominant around Makurdi, Akwana, Akiri, and Wukari.

Mineralization associated with thorium includes basement granitic rocks, migmatite, shales, and clay. Again, Uranium concentration is a high concentration of Uranium around Lafia, Akiri, Ibi, Akwana, south of Wukari, and Makurdi north. A low concentration of U is found around Kwolla, Shendam, Wamba, Wukari, and Makurdi south. Shales, clay, and basement complex rocks (such as granite and migmatite) are associated with uranium mineralization.

Based on the results obtained, the areas with a high concentration of radiometric heat, low Curie point depth; high geothermal gradient, and high geothermal heat flow are the hot spots for geothermal energy potential in the investigated area. Geologically, these areas are those covered by basement complex, volcanic intrusives; and sandstones and shales (in the sedimentary area). Based on these thicknesses range, the possibility of hydrocarbon generation is viable in the area if every other condition for hydrocarbon accumulation is positive.

6 References

Abraham, E. M., Obande, E. G., Chukwu, M., Chukwu, C. G. and Onwe, M. R., 2015, Estimating depth to the bottom of magnetic sources at Wikki Warm Spring region, N.E. Nigeria, using fractal distribution of sources approach, Turkish Journal of Earth Sciences, vol. 24, pp 1-19.

Abraham, E. M. and Nkitnam, E. E., 2017, Review of Geothermal Energy Research in Nigeria: The Geoscience Front, International Journal of Earth Science and Geophysics, vol. 3, No. 15, pp. 1-10.

Anudu, G. K., Stephenson, R. A. and Macdonald, D. I. M., 2014, Using high-resolution aeromagnetic data to recognize and map intra-sedimentary volcanic rocks and geological structures across the Cretaceous Middle Benue Trough, Nigeria, Journal of African Earth Sciences, vol. 99, pp. 625-636.

Bansal, A. R., Anand, S. P., Rajaram, M., Rao, V. K., Dimri, V. P., 2013, Depth to the bottom of magnetic sources (DBMS) from aeromagnetic data of Central India using modified centroid method for fractal distribution of sources, Tectonophysics, vol. 603, pp 155-161.

Beamish, D. and Busby, J., 2016, The Corrubian geothermal province: Heat production and flow in South-Western England: estimates from boreholes and airborne gamma-ray measurements, Geothermal Energy, vol. 4, No. 4, pp. 1-25.

Bello, R., Ofoha, C. C. and Wehiuzo, N., 2017, Geothermal Gradient, Curie Point Depth and Heat Flow Determination of some Pats of Lower Benue Trough and Anambra Basin, Nigeria, using High-Resolution Aeromagnetic Data, Physical Science International Journal, vol. 15, No. 2, pp. 1-11.

Benkhelil, I., 1989, The origin and evolution of the Cretaceous Benue Trough, Nigeria, Journal of African Earth Sciences, vol. 8, pp. 251-282.

Bhattacharyya, B. K. and Leu, L. K., 1975, Analysis of magnetic anomaly over Yellowstone National Park: Mapping of Curie point isothermal surface for geothermal reconnaissance, Journal of Geophysical Research, vol. 8, pp.4461-4465.

Biswas, A., Parija, M. P., Kumar, S., 2017, Global nonlinear optimization for the interpretation of source parameters from total gradient of gravity and magnetic anomalies caused by thin dyke. Annals of Geophysics, 60 (2), G0218, pp 1-17

Blakely, R. J., 1988, Curie temperature isotherm analysis and tectonic implications of aeromagnetic data from Nevada, Journal of Geophysical Research, vol. 93, pp. 11817-11832.

Burke, K. C., Dessauvagie, T. F. J.,

Whiteman, A. J., 1972, Geological history of the Benue valley and adjacent areas. In: Dessauvagie, T.F.J, Whiteman, A.J. (Eds), African Geology, University of Ibadan, Ibadan, pp. 181-185.

Burke, K. C. and Whiteman, A. J., 1973, Uplift, rifting and the break-up of Africa. In: Tarling, D.H., Runcorn, S.K. (Eds), Implications on Continental Drift to Earth Sciences, pp. 735-755.

Cratchley, C. R. and Jones, G. P., 1965, An interpretation of geology and gravity anomalies of the Benue Valley, Nigeria, Overseas Geological Survey, London, Geophysics, Paper No. 1.

Davis, J. C., 1972, Statistics and Data Analysis in Geology, John Wiley and Sons, New Delhi, India, 638p.

Ikechukwu, I. O., Agbidi, D. C. and Olusola, O. B., 2015, Exploration and Application of geothermal energy in Nigeria, International Journal of Scientific and Engineering Research, vol. 6, No. 2, pp. 726-732.

Kasidi, S. and Nur, A., 2013, Estimation of Curie point depth, Heat flow and Geothermal gradient inferred from aeromagnetic data over Jalingo and Environs, -Eastern Nigeria, International Journal of Science and Emerging Technologies, vol. 6, No. 6, pp. 294-301.

Likkason, O. K., 1993, Application of trend surface analysis of gravity data over the Middle Niger Basin, Nigeria, Journal of Mining and Geology, vol.6 No. 2, pp.11-19.

NGSA, 2009, Nigerian Geological Survey of Agency: Geology of the Benue Trough. .

Nwankwo, L. I. and Shehu, A. T., 2015, Evaluation of Curie-point depths, geothermal gradients and near–surface heat flow from high-resolution aeromagnetic (HRAM) data of the entire Sokoto Basin, Nigeria, Journal of Volcanology, Geothermal Research, vol. 305, pp. 45-55.

Nwankwo, L. I. and Abayomi, J. S., 2017, Regional estimation of Curie-point depths and succeeding geothermal parameters from recently acquired high-resolution aeromagnetic data of the entire Bida Basin, North-Central Nigeria, Geothermal Energy Science, vol. 5, pp. 1-9.

Obaje, N. G., Wehner, H., Hamza, H. and Scheeder, G., 2004, New Geothermal data from the Nigerian sector of the Chad Basin: Implications on hydrocarbon Prospectivity, Journal of African Earth Sciences, vol. 38, No.5, pp. 477-487.

Obaje, N. G., 2009, Geology and Mineral Resources of Nigeria, Lecture Notes in Earth Sciences, Springer, Berlin Heidelberg.

Ochieng, L., 2013, Overview of geothermal surface exploration methods, presented at short course VIII on exploration for geothermal resources, organised UNU-GTP, GDC and Ken-Gen, at lake Naivasha, Kenya, October 31st - November 22nd, 2013.

Offodile, M. E., 1976, The geology of Middle Benue Trough, Nigeria, Special volume of Paleontological Institute, University of Uppsala, vol. 4, pp. 1-66.

Offodile, M. E., 1980, A mineral survey of the cretaceous of the Benue Valley, Nigeria, Cretaceous Resource, vol.1, pp.101-124.

Offodile, M. E., 1989, A Review of the geology of the Cretaceous of the Benue Valley. In: Kogbe, C.A. (Ed), Geology of Nigeria (Second Revised Edition), Rock View Nigeria Limited, Jos, 538p.

Okubo, Y., Graff, R. G., Hansen, R. O., Ogawa, K. and Tsu, H., 1985, Curie point depths of the Island of Kyushu and Surrounding areas, Geophysics, vol. 53, pp. 481- 494.

Ojonugwa, A.U, Ezeh, C.C, Chinwuko, I.A 2018, Integration of Aeromagnetic Interpretation and Induced Polarization Methods in Delineating Mineral Deposits and Basement Configuration within Southern Bida Basin, North-

West Nigeria. J Geol Geophys 7: 449.
Ross, H. E., Blakely, R. J. and Zoback, M. D., 2006, Testing the use of aeromagnetic data for the determination of Curie depth in California, Geophysics, vol. 71, pp. 51-59.
Salako, K. A., Adetona, A. A., Rafiu, A. A., Alahassan, U. D., Aliyu, A. and Adewumi, T., 2020, Assessment of Geothermal Potential of Parts of Middle Benue Trough, North-East Nigeria. Journal of the Earth and Space Physics, Vol. 45, No. 4, Winter 2020, P. 27-42
Salem, A. and Fairhead, D., 2011, Geothermal reconnaissance of Gebel Dui area, Northern Red Sea, Egypt, using airborne magnetic and spectral gamma ray data, Getech, pp. 1-22.
Sedara, S. O. and Joshua, E. O., 2013, Evaluation of the Existing State of Geothermal Exploration and Development in Nigeria, Journal of Advances Physics, vol. 2, No. 2, pp. 118-123.
Stampolidis, A., Kane, I., Tsokas, G. N. and Tsourlos, P., 2005, Curie point depths of Albania inferred from ground total field magnetic data, Surveys in Geophysics, vol. 26, pp. 461-480.
Tanaka, A. Y., Okubo, Y. and Matsubayashi, O., 1999, Curie point depth based on spectrum analysis of the magnetic anomaly data in East and Southeast Asia, Tectonophysics, vol. 396, pp. 461-470.
Telford, W. M., Geldart, I. P. and Sheriff, R. E., 1990, Applied Geophysics, Second Edition, Springer, Berlin, 770p.
Yamano, M., 1995, Recent heat flow studies in and around Japan, In: Gupta, M.I. and Yamano, M. (eds), Terrestrial Heat Flow and Geothermal Energy in Asia, A.A. Balkema, Rotterdam, pp. 171-200.